Code Comparison Project – two-layer setup 3D simulation (RANS analysis hightlights)

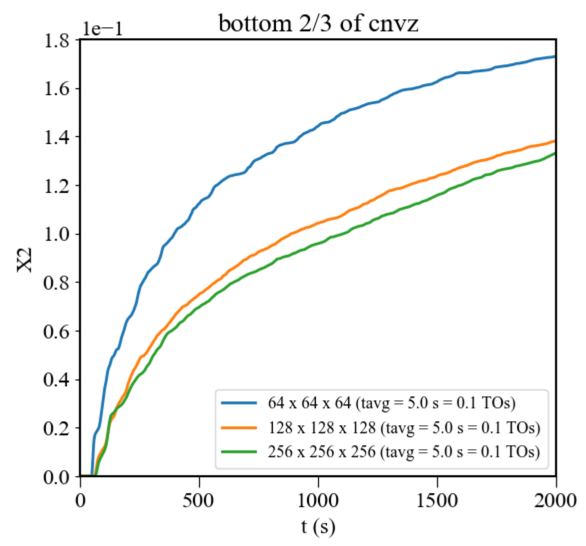

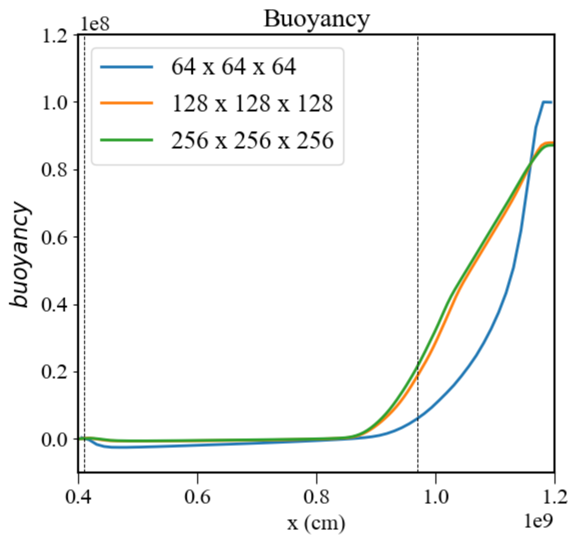

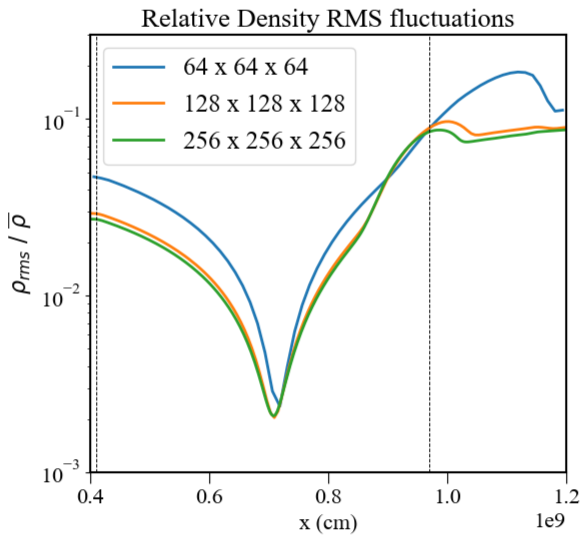

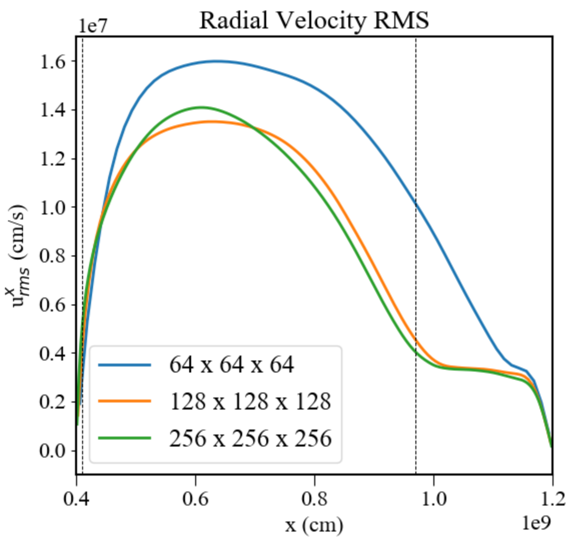

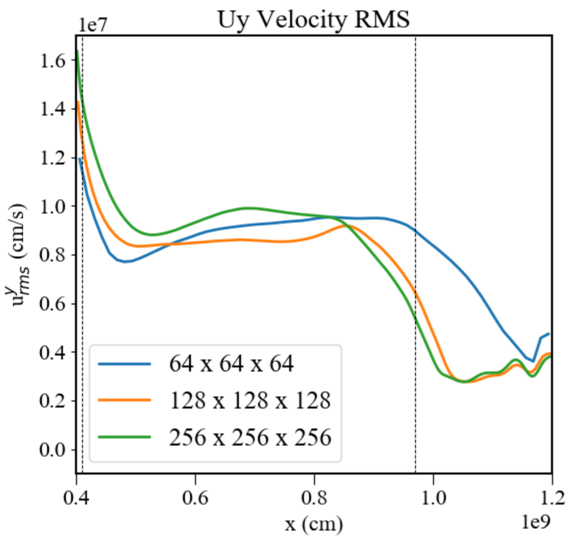

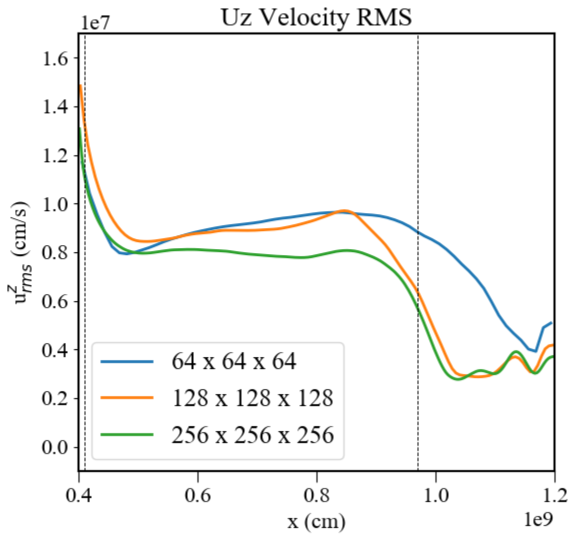

With increasing resolution, the entrainment rate decreases. This is consistent with Woodward , 2014. The strength of turbulence at convection boundary decreases (the radial and horizontal rms velocity goes down, perhaps due to decreasing density fluctuations >> less buoyancy >> weaker turbulence flow).Does the boundary become stiffer?Can you infer from buoyancy jump?What effect has averaging window tavg? above averaged over 1500 s.

One of the primary conclusions of these studies is that the entrainment rate depends on a Richardson number, which is a dimensionless measure of the "stiffness" of the boundary relative to the strength of the turbulence. In shear-free turbulent entrainment the bulk Richardson number,

$$\mathrm{Ri}_B = \frac{\Delta b L}{\sigma^2}, \tag{2}$$

is most commonly studied. Here Δb is the buoyancy jump across the interface, σ is the rms turbulence velocity adjacent to the interface, and L is a length scale for the turbulent motions, which is often taken to be the horizontal integral scale of the turbulence near the interface. The relative buoyancy is defined by the integral

$$b(r) = \int_{r_i}^{r} N^2\, dr, \tag{3}$$

where N is the buoyancy frequency defined by

$$N^2 = -g\left(\frac{\partial \ln \rho}{\partial r} - \frac{\partial \ln \rho}{\partial r}\bigg|_s\right). \tag{4}$$

The entrainment coefficient E is the interface migration speed u_e normalized by the rms turbulent velocity at the interface $E = u_E/\sigma$ and is generally found to obey a power-law dependence on Ri_B,

$$E = A\mathrm{Ri}_B^{-n}. \tag{5}$$

The exponent is usually found to lie in the range $1 \lesssim n \lesssim 1.75$

CASEY A. MEAKIN[1,2] AND DAVID ARNETT[1]
Received 2006 October 27; accepted 2007 May 21

PAUL R. WOODWARD[1], FALK HERWIG[2], PEI-HUNG LIN
Submitted: July 15, 2013; Accepted: August 12, 2014

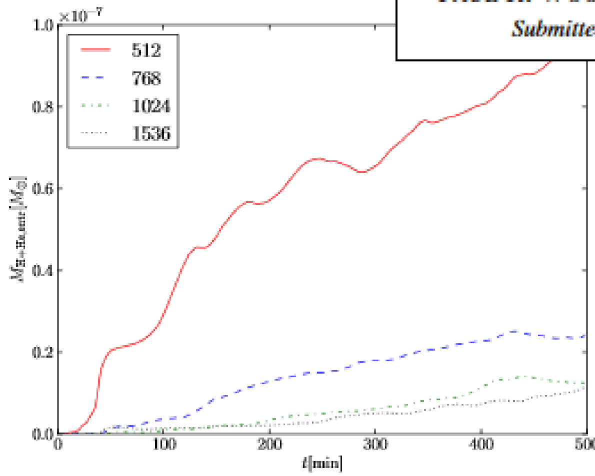

FIG. 16.— Entrained mass, integrated between the radial coordinates 10100km and 29200km, as a function of time. Simulations for different grid sized n^3 are shown. The number of grid points n in one direction is shown in the legend.

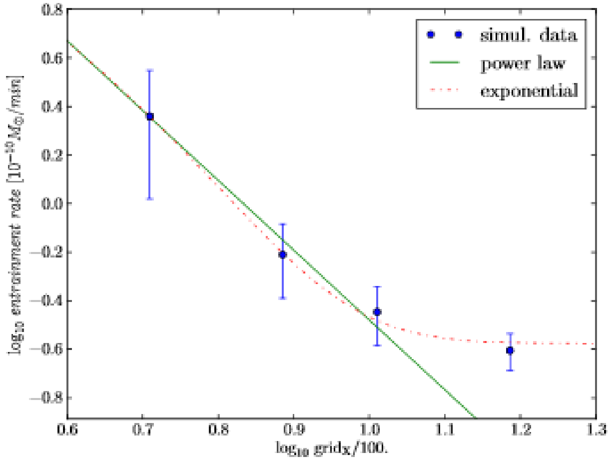

FIG. 17.— Logarithm of mean entrainment rates with error bars representing 99% confidence intervals (see text) as a function of grid size. The mean entrainment rates have been fitted with a power law and an exponential according to Eq. (7).

Turbulent kinetic energy dissipation appear to play a significant role at controling internal energy, temperature or enthalpy evoluti. See below epsilon terms

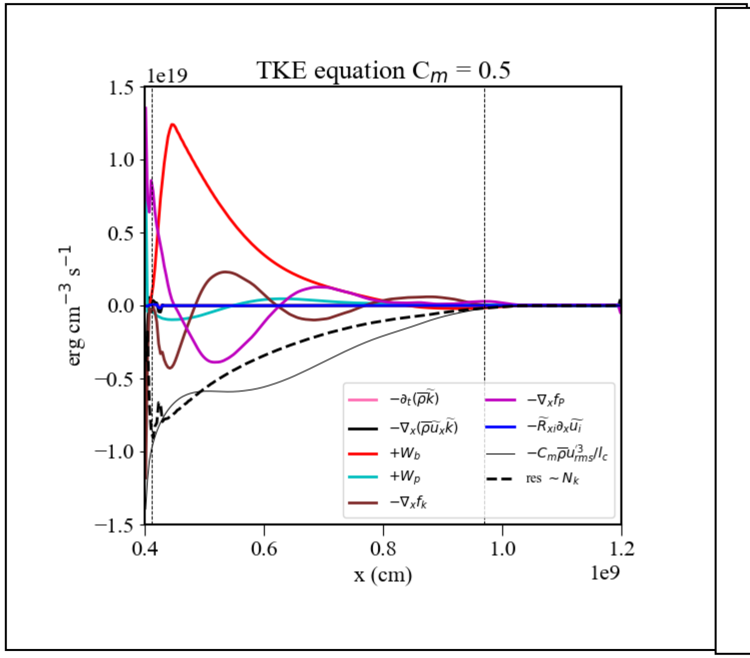

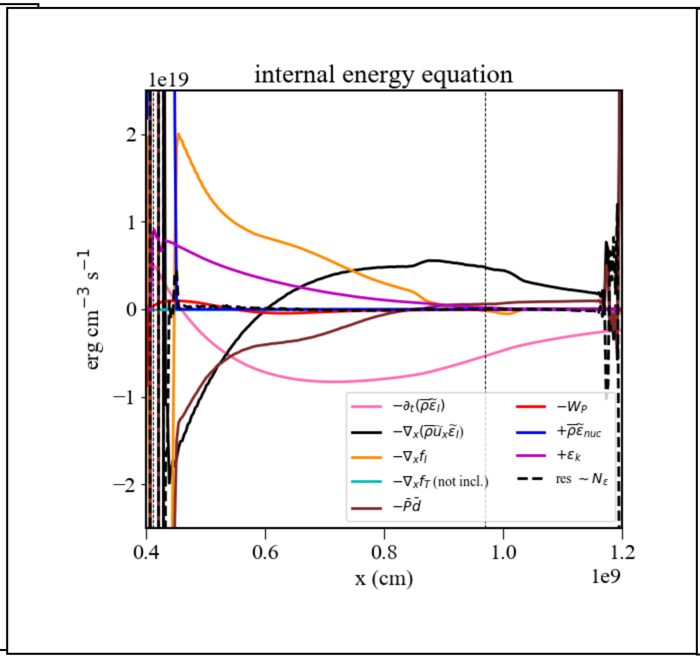

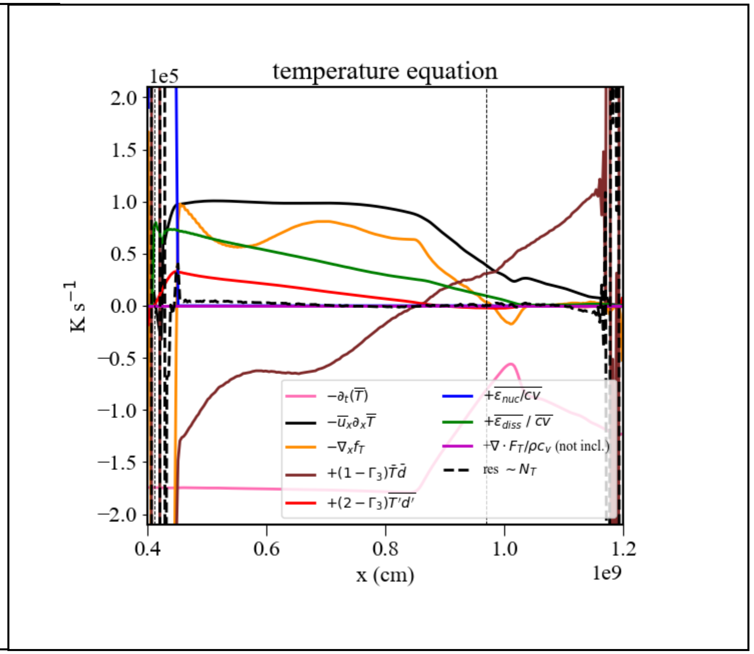

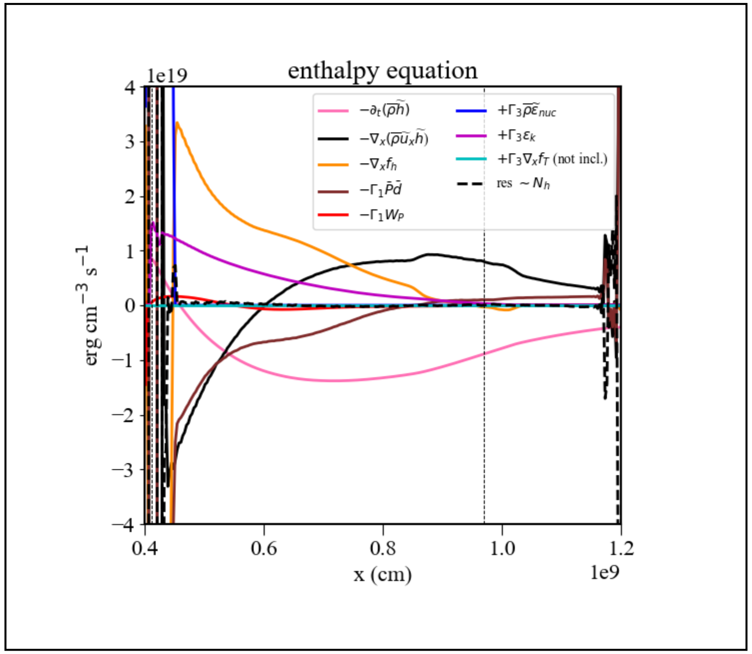

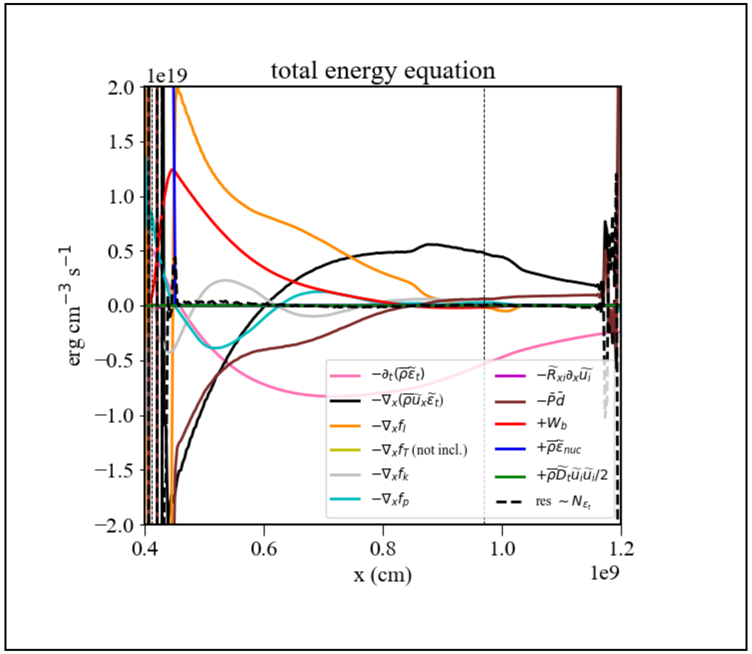

Occasional burst of relatively large res when averaging over many TOs – below the cont eq. res from 256 cubed, intc 110, one of the first spikes in the plots

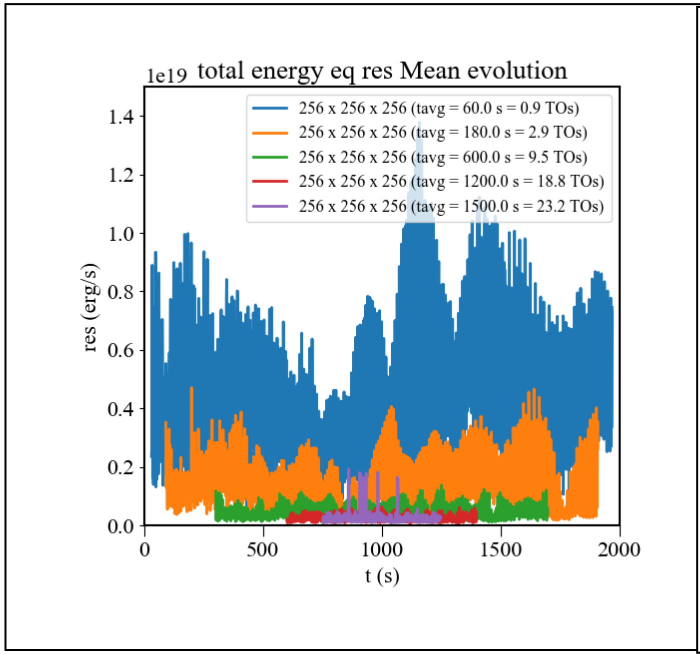

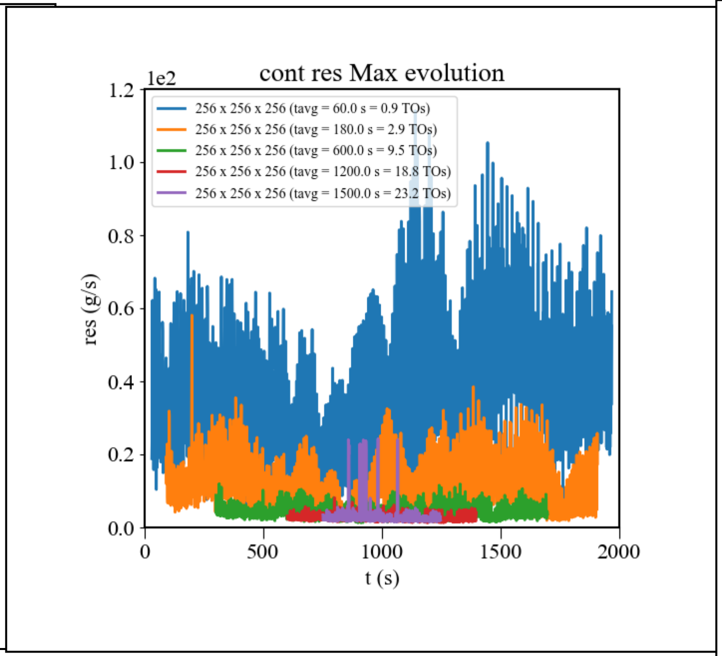

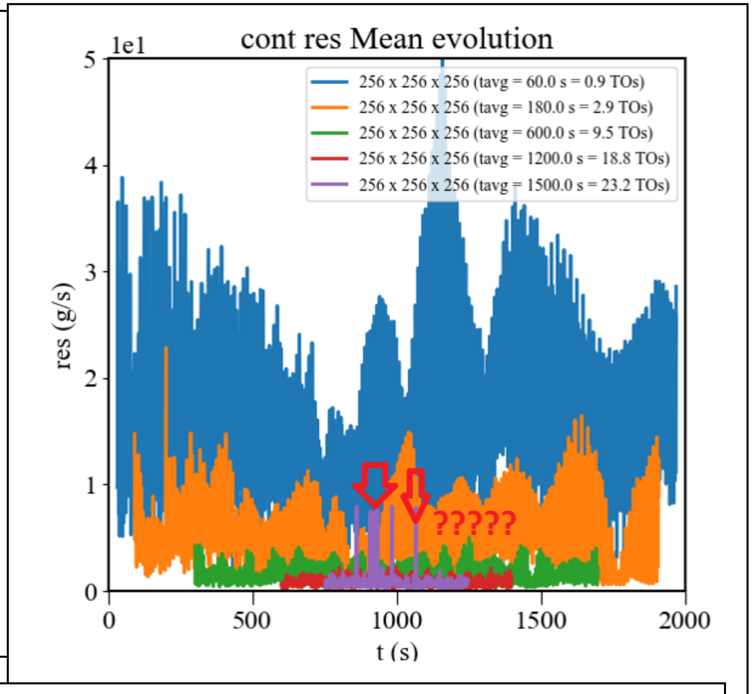

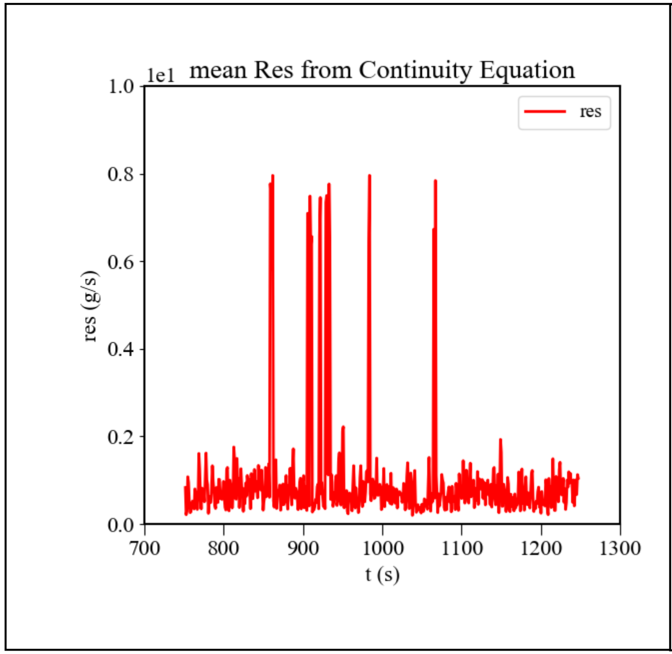

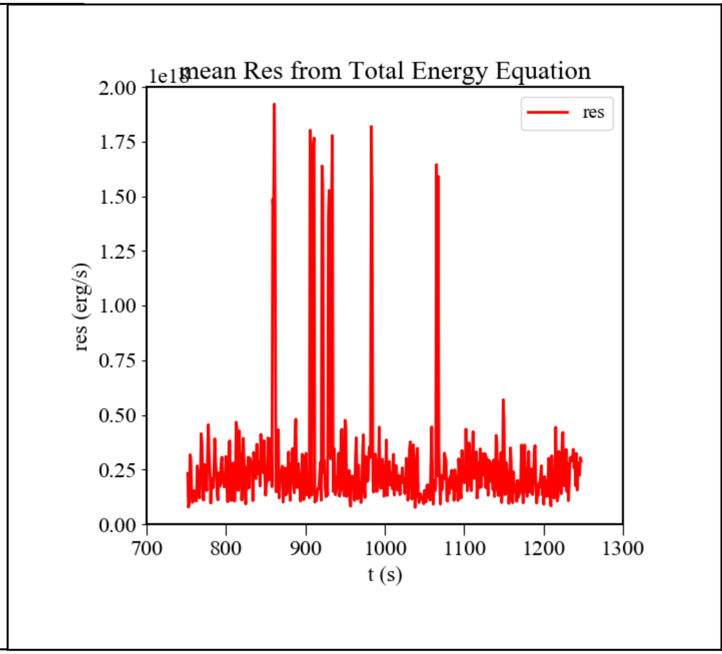

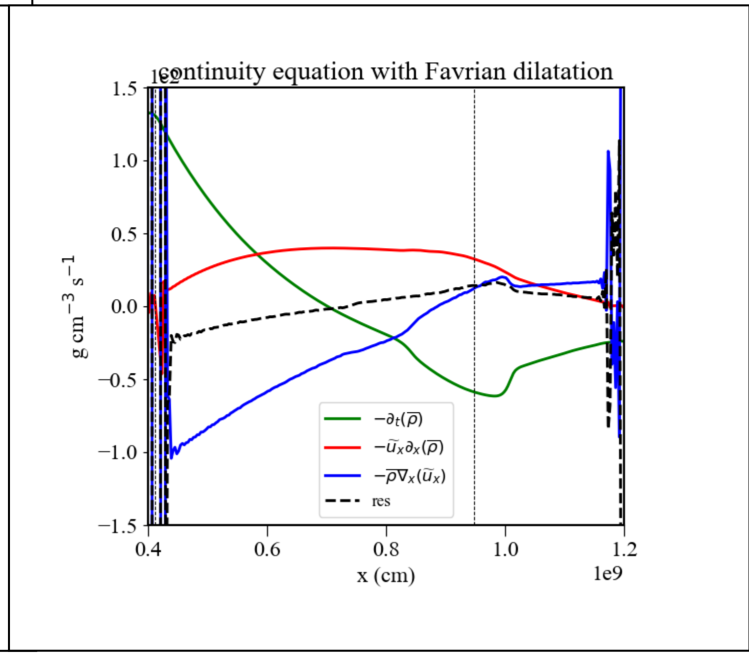

Dependence of RANS on averaging window: - (below tavg 180 secs – 3 TOs, 600 secs – 10 TOs, 1500 secs – 25 TOs at timec = 1017 secs) – LOOKS LIKE AVERARGING OVER 3 TOs not enough, the 25 Tos averaging window gives best residual. The mean fields change visible at convection bndry mostly.

180 secs (3 TOs) 600 secs (10 TOs) 1500 secs (25 TOs)

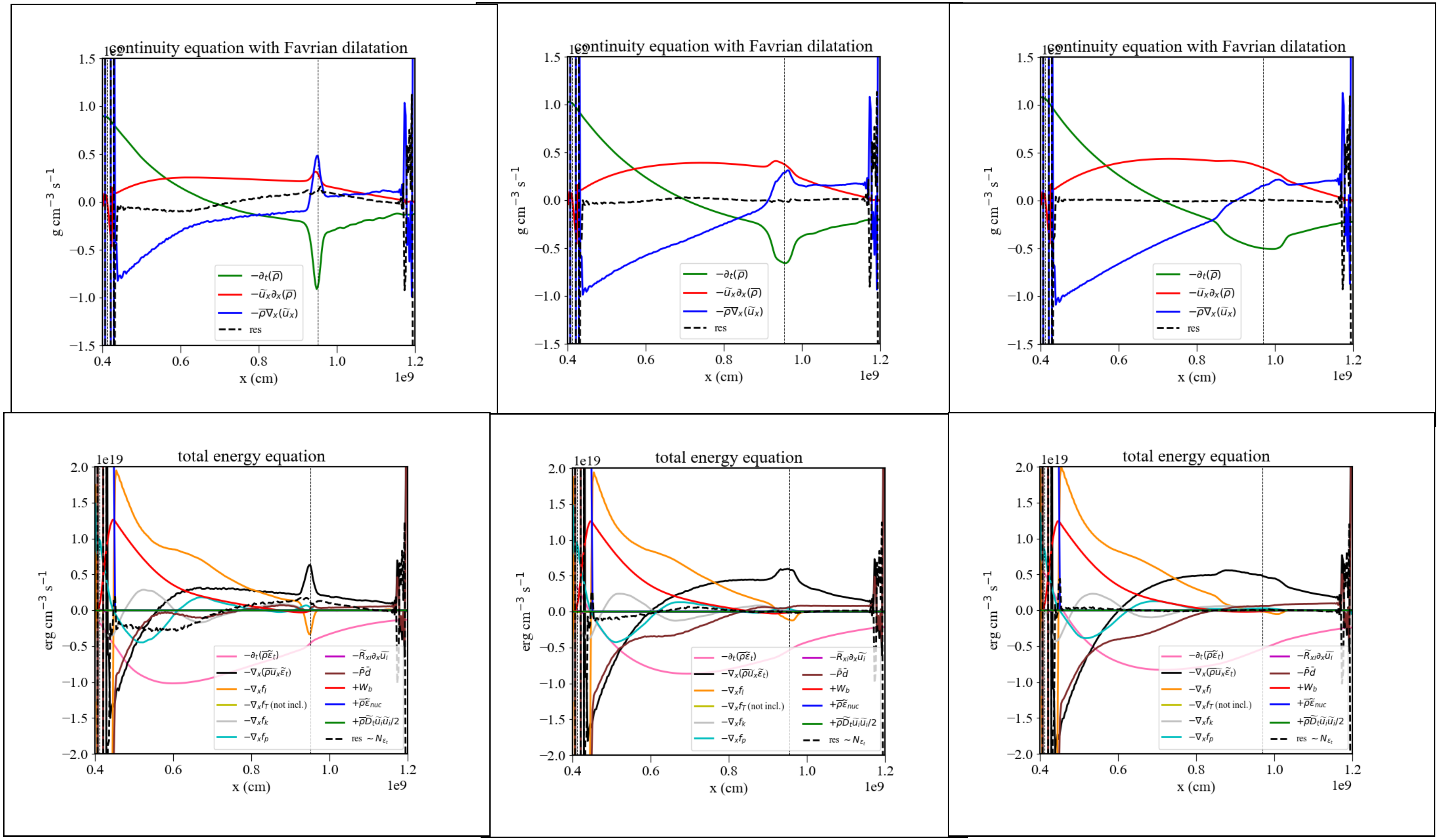

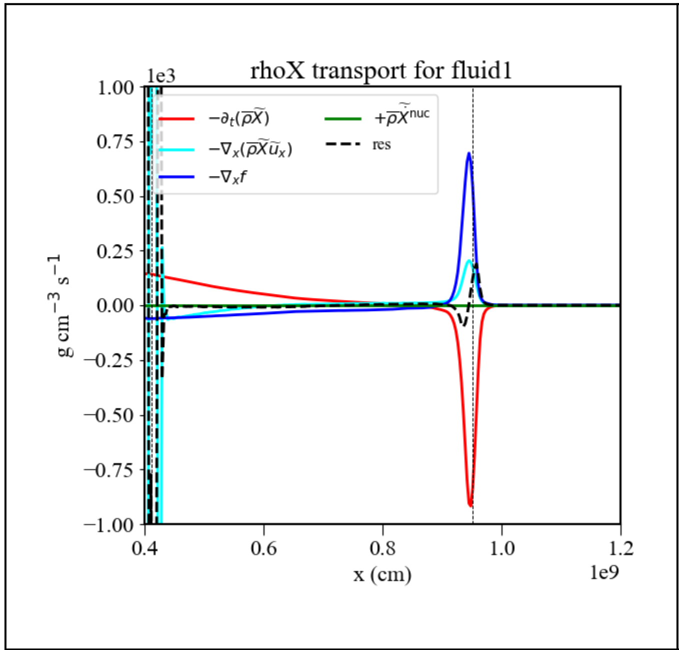
rhoX transport for fluid1
1e3
$-\partial_t(\overline{\rho}\widetilde{X})$
$-\nabla_x(\overline{\rho}\widetilde{X}\widetilde{u}_x)$
$-\nabla_x f$
$+\overline{\rho}\widetilde{\dot{X}}^{\rm nuc}$
res
g cm^{-3} s^{-1}
x (cm)
1e9

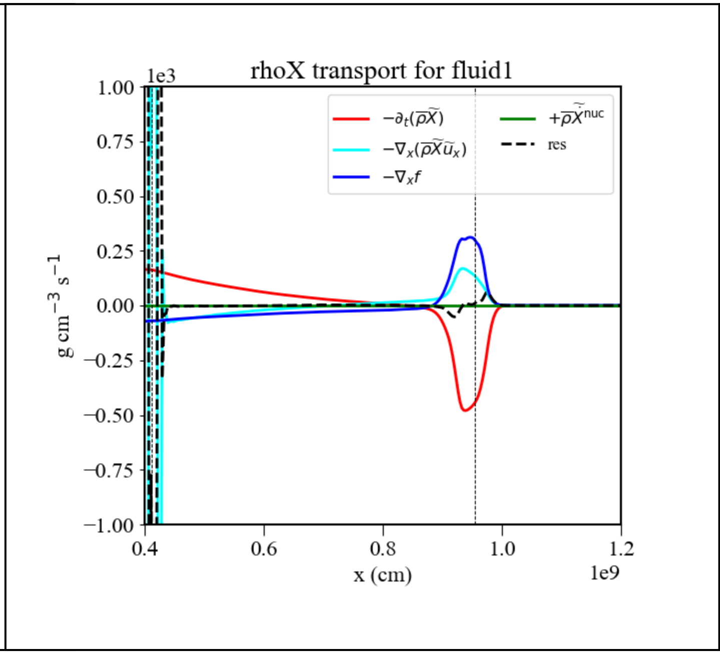
rhoX transport for fluid1
1e3
$-\partial_t(\overline{\rho}\widetilde{X})$
$-\nabla_x(\overline{\rho}\widetilde{X}\widetilde{u}_x)$
$-\nabla_x f$
$+\overline{\rho}\widetilde{\dot{X}}^{\rm nuc}$
res
g cm^{-3} s^{-1}
x (cm)
1e9

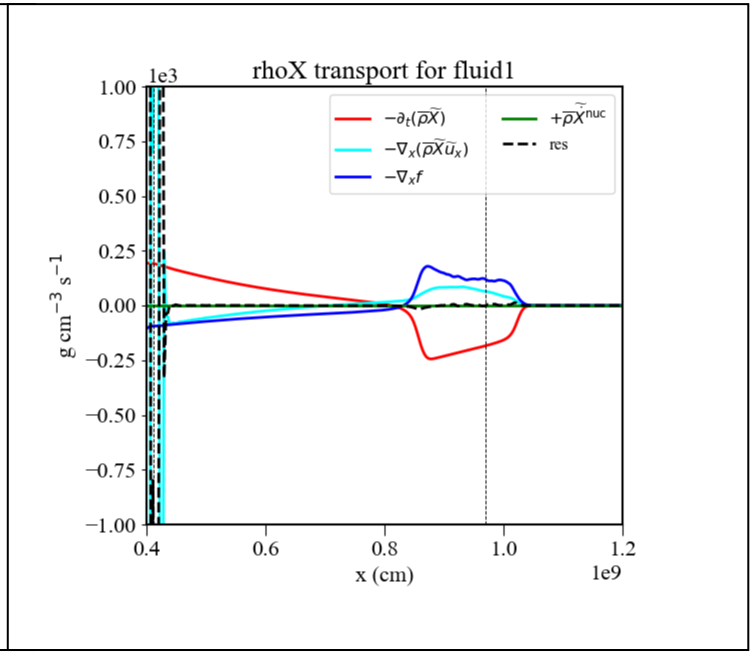
rhoX transport for fluid1
1e3
$-\partial_t(\overline{\rho}\widetilde{X})$
$-\nabla_x(\overline{\rho}\widetilde{X}\widetilde{u}_x)$
$-\nabla_x f$
$+\overline{\rho}\widetilde{\dot{X}}^{\rm nuc}$
res
g cm^{-3} s^{-1}
x (cm)
1e9

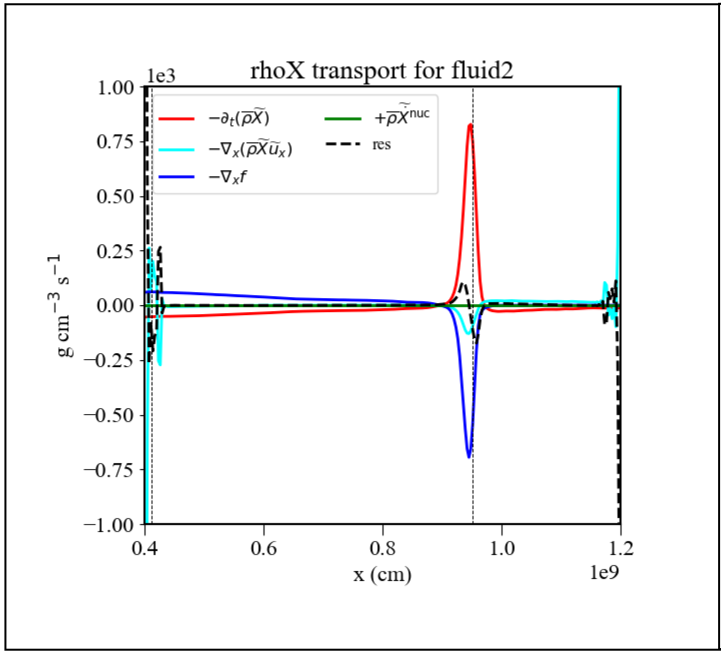
rhoX transport for fluid2
1e3
$-\partial_t(\overline{\rho}\widetilde{X})$
$-\nabla_x(\overline{\rho}\widetilde{X}\widetilde{u}_x)$
$-\nabla_x f$
$+\overline{\rho}\widetilde{\dot{X}}^{\rm nuc}$
res
g cm^{-3} s^{-1}
x (cm)
1e9

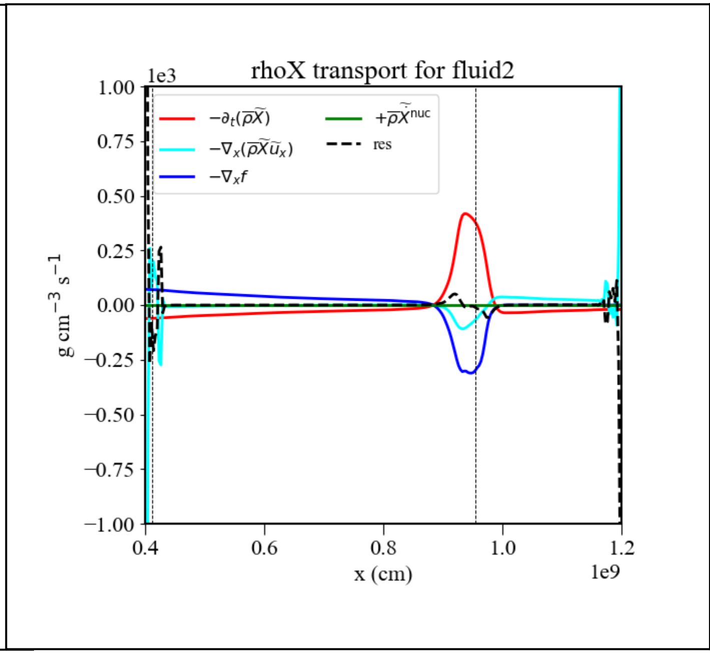
rhoX transport for fluid2
1e3
$-\partial_t(\overline{\rho}\widetilde{X})$
$-\nabla_x(\overline{\rho}\widetilde{X}\widetilde{u}_x)$
$-\nabla_x f$
$+\overline{\rho}\widetilde{\dot{X}}^{\rm nuc}$
res
g cm^{-3} s^{-1}
x (cm)
1e9

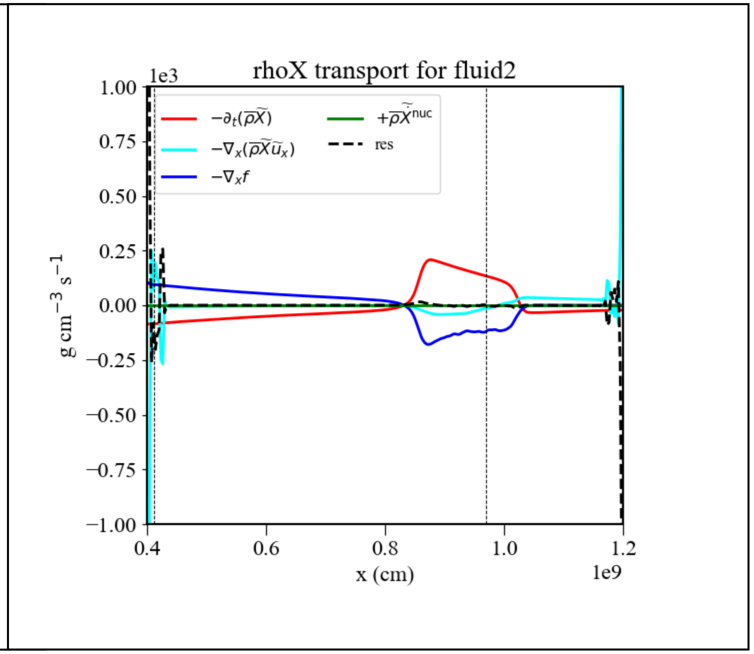
rhoX transport for fluid2
1e3
$-\partial_t(\overline{\rho}\widetilde{X})$
$-\nabla_x(\overline{\rho}\widetilde{X}\widetilde{u}_x)$
$-\nabla_x f$
$+\overline{\rho}\widetilde{\dot{X}}^{\rm nuc}$
res
g cm^{-3} s^{-1}
x (cm)
1e9

Dependence of turbulence velocities, Mach numbers as a function of luminosity

T.B.D

3D hydrodynamic simulations of C ingestion into aconvective O shellR. Andrassy,[1,2,3?]F. Herwig,[1,2]P. Woodward,[4,2]C. Ritter[1,2]

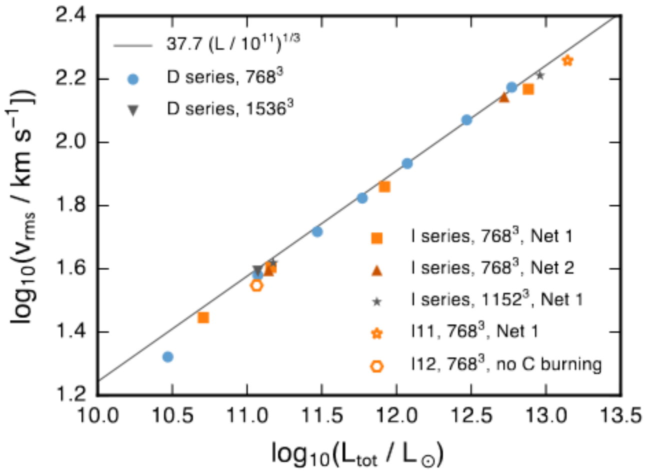

Figure 15. Dependence of the rms convective velocity $v_{\rm rms}$ on the total luminosity $L_{\rm tot}$ integrated over the convection zone. The expected scaling law $v_{\rm rms} \propto L_{\rm tot}^{1/3}$ is shown for comparison. The last 2.2 min of run I11 are used when the instability described in Sect. 3.6 has fully developed.